NRC Research Press

ARTICLE

Ductility and durability enhancement of concrete EPS by new reinforcement arrangements and polypropylene FRC utilization

Tae-Kyun Kim, Hoo-Bum Lee, Tae-Hee Lee, Seung-Jai Choi, and Jang-Ho Jay Kim

Abstract: The majority of precast concrete electric pole structures (EPSs) consist of prestressed concrete and reinforced concrete hybrid members with high slenderness ratios. Currently, large prestressing (PS) forces are being applied to EPSs to carry heavier weights of electric transformer machineries and to reduce deflection by increasing structural stiffness. Moreover, when EPSs are exposed to an outdoor environment year-round, their durability decreases. Therefore, the objectives of this study are to transform the failure behavior of EPSs from brittle to ductile by varying the number of PS tendons and steel rebars, and to improve the ductility and durability of the EPS by using short polypropylene fiber-reinforced concrete to control crack formation and propagation. Six different types of EPS specimens were manufactured and tested to evaluate their maximum flexure capacity and to verify their ductility behavior. The results showed that the modified EPSs displayed ductile failure behavior while either maintaining their original flexural strength capacity or improving it compared with the current EPSs sold on the market.

Key words: electrical pole structures, prestressed concrete, fiber-reinforced concrete, ductility, durability, flexural strength.

Résumé : La majorité des structures de poteaux électriques (SPE) en béton précontraint sont constituées de béton précontraint et d'éléments hybrides en béton armé ayant des rapports d'élancement élevés. Actuellement, de grandes forces de précontrainte sont appliquées aux SPE pour supporter des poids plus lourds de transformateurs électriques et pour réduire la déformation en augmentant la rigidité structurelle. De plus, lorsque les SPE sont exposés à un environnement extérieur toute l'année, leur durabilité diminue. Par conséquent, les objectifs de cette étude sont de transformer le comportement de défaillance des SPE de fragile à ductile en faisant varier le nombre d'armatures de précontrainte et de barres d'armature en acier, et d'améliorer la ductilité et la durabilité des SPE en utilisant du béton renforcé de fibres courtes en polypropylène pour contrôler la formation et la propagation de fissures. Six types différents de modèle de SPE ont été fabriqués et mis à l'essai afin d'évaluer leur capacité de flexion maximale et de vérifier leur comportement en matière de ductilité. Les résultats ont montré que les SPE modifiés affichaient un comportement de défaillance ductile tout en maintenant leur capacité initiale de résistance à la flexion ou en l'améliorant par rapport aux SPE actuels vendus sur le marché. [Traduit par la Rédaction]

Mots-clés : structures de poteaux électriques, béton précontraint, béton renforcé de fibres, ductilité, durabilité, résistance à la flexion.

Introduction

Most electric pole structures (EPSs) that are presently manufactured contain a hybrid combination of prestressed concrete (PSC) and reinforced concrete (RC) (Xu et al. 2018; Saatcioglu and Yalcin 2003). EPSs are categorized into light, medium, and heavy types, which can carry 5, 7, and 10 kN axial loads, respectively. As EPSs consist of the PSC–RC hybrid member, their collective strengths are improved by prestressing tendons in a longitudinal direction. Typical examples of PSC structures include liquefied natural gas (LNG) tanks and nuclear containment vessels. These tanks and vessels are built by prestressing high strength concrete (HSC) to generate a maximum confinement effect, thereby increasing the PSC–RC member's load-bearing capacity (Soltani et al. 2013; Shanaka et al. 2018; Lee and Billington 2007). However, the EPSs' prestressed (PS) confining force is only generated longitudinally, thereby lowering their effectiveness in applying lateral confining stress.

HSC is commonly used in manufacturing PSC structures due to its excellent material properties, such as abrasion resistance, compressive strength, and crack resistance (Janke et al. 2009; Phan et al. 2012; Ali et al. 2010. However, one drawback of the HSC EPS is that it is applied with excessive prestressing force to maximize its weight-to-load carrying capacity. Additionally, due to HSC's inherent brittle macrocrack inducing characteristic, HSC EPS is vulnerable to catastrophic rupture failure (Nathan 1985; Rodriguez-Gutierrez and Aristizabal-Ochoa 2001*a*). Furthermore, due to its high slenderness ratio and brittle fracturing characteristics, catastrophic failures can occur (Wolanski 2004; Rodriguez-Gutierrez and Aristizabal-Ochoa 2001*b*; Kim et al. 2010). Catastrophic failures of EPSs can lead to serious human casualties and property damage. Moreover, when cracks form in aged EPSs, moisture penetrates into the structure through the cracks, causing cyclic freeze–thaw damage in the member; this damage then leads to corrosion in the rebars and PS tendons (Arya and Darko 1996; Audenaert et al. 2009). Additionally, when concrete begins to lose

Received 26 March 2019. Accepted 2 December 2019.

T.-K. Kim, H.-B. Lee, T.-H. Lee, S.-J. Choi, and J.-H.J. Kim. School of Civil and Environmental Engineering, Yonsei University, 50 Yonsei-Ro, Seodaemun-Gu, Seoul 03722, Republic of Korea.

Corresponding author: Jang-Ho Jay Kim (email: jjhkim@yonsei.ac.kr).

its alkalinity, it reacts with the carbon dioxide in the air to accelerate the corrosion process (Jung et al. 2010; Xi et al. 2018). When these aged EPSs are subjected to wind gust and impact loads they can easily experience catastrophic failure (Vivek et al. 2017; Xu et al. 2018). Due to problems associated with the current EPSs sold on the market, a need for studies on their reinforcement and concrete improvements first emerged in the early 1990s. However, in-depth studies and detailed design enhancements are still lacking, even at present.

Steel fibers (SF) or plastic fibers (PF) are commonly added to concrete mixes to produce fiber-reinforced concrete (FRC). For PF, short PF fibers with lengths of 20–50 mm are usually added into the concrete mix. Among all short plastic fibers sold on the market, polypropylene (PP) fibers are the most widely used in concrete members due to its low price. To improve the bonding between PP fibers and the concrete matrix, a surface shape modification of PP fibers, such as embossing or twisting, is required. PP fibers have a low melting point and a more elastic coefficient than other fibers, but its high tensile strength, chemical resistance, and alkali resistance increase the durability of the concrete. The fibers mixed in the concrete serve to bridge the cracks for stress transfers across the microcracks. This crack bridging ability increases the tensile and bending strengths of FRC, thereby enhancing the overall load-bearing capacity, ductility, shear strength, and impact resistance of the concrete members (Thompsin and Park 1980).

In this study, to deal with the aging problem of EPSs, various reinforcement arrangement types and FRC usage are proposed for manufacturing new concrete EPSs. The objective of this study is to change the brittle failure behavior of conventional EPSs to a ductile failure behavior and to improve its durability capacity. To evaluate the performance of the newly proposed EPSs, new EPSs with short PP FRC and various reinforcement arrangements are manufactured. Then, real scale flexural pull tests are conducted to evaluate the EPSs' structural performance. The study results are discussed in detail and conclusions are presented.

Current and new EPS reinforcement arrangements

Reinforcement arrangements of current EPSs

Currently, EPSs sold on the market are categorized into light, medium, and heavy-capacity types, which have 8 PS tendons (Ø 9.2 mm) with 8 rebars (Ø 8 mm), 8 tendons with 8 rebars (Ø 11 mm), and 8 tendons (Ø 13 mm) with 8 rebars (Ø 13 mm), respectively. Spiral lateral reinforcement is applied using 3 mm steel wire at 9 mm spacing. PS forces of 520, 730, and 1010 kN were applied to light, medium, and heavy-capacity EPSs, respectively. The reinforcement details of current EPSs are listed in Table 1. As excessive prestressing of EPSs can lead to brittle catastrophic failure, EPS failure behavior conversions from brittle to ductile failures were attempted by adjusting the number and size of PS tendons and rebars.

EPS specimen dimensions and material properties

The dimensions of the EPS specimens used in this study are shown in Fig. 1. The concrete mix design and tendon and rebar properties are listed in Tables 2 and 3, respectively. The concrete mix designs for the light, medium, and heavy EPSs shown in Table 2 are the same mix designs used to cast conventional EPSs, except for an addition of a 0.3% PP fiber volume ratio (Table 4). However, a different mix design using a concrete strength of 120 MPa is used to manufacture heavy EPSs and, thereby, drastically improve its load-carrying capacity. Even with this updated mix design, the 0.3% PP fiber volume ratio is consistent with the other previous mix designs. The rebar and tendon properties listed in Table 3 are the properties of normal-strength steel rebars and tendons used to manufacture conventional EPSs.

Table 1. Tendon and rebar arrangements of control EPS specimen.

Capacity type	Tendon size (mm)	No. used	Rebar size (mm)	No. used
Light	9.2	8	8	8
Medium	11	8	11	8
Heavy	13	8	13	8

Specimen preparation and manufacturing

In manufacturing EPS specimens, the centrifugal casting method was used. Assembled PC tendons and reinforcements were placed in the formwork and the PS tendons were subjected to tension. After pouring concrete, the formwork was finally assembled and compacted by centrifugal force so that the thickness of the pole was uniform. Then, the specimens were initially steam cured for one day, followed by air curing for 27 days. One batch was mixed and casted for each EPS series at the same time. The light, medium, heavy 1, heavy 2, heavy 3 capacity mix types shown in Table 5 developed compressive strength over the same 28 day period within an error margin.

When PP FRC is manufactured using a spinning wheel, PP fibers tend to move toward the outer surface region of an EPS due to the centrifugal momentum effect. As the majority of fibers are located at the outer surface regions of EPSs, the fibers are more effective in increasing the durability of EPSs by controlling their surface microcracks.

Fiber-reinforced concrete for durability improvement

Conventional EPSs are manufactured using HSC with a designed compressive strength of 50 MPa (KS F 4304). When cracks and damage occur in an EPS due to service aging, its concrete cover can spall off, which leads to secondary damage. To minimize the cracking and damage problems of the concrete cover, addition of short plastic fibers to the concrete is proposed. FRC is applicable to structural members as well as non-structural members, which significantly increases the durability of the concrete structures (Castoldi et al. 2019). The service lives of structures exposed to external environments, such as EPSs, can be extended by improving their crack resistance and overall durability by using short plastic fibers. Moreover, since the shear strength can be improved by using FRC, as FRC is an effective material for PSC and RC structures requiring a high shear capacity (Hwang et al. 2016). FRC can improve EPS ductility by controlling microcrack formation.

Since the tensile and bending strengths of PP FRC increase in proportion to the mixing ratio, an optimum volume percentage of PP fibers in FRC mixes used to cast EPS must be determined. To determine this percentage, PP fiber mixing ratios of 0.3%, 0.5%, and 0.7% were used in the FRC mix design to manufacture current medium capacity EPSs sold on the market. PS forces of 510, 420, and 630 kN were applied to the light, medium, and heavy-capacity EPSs, respectively. Table 4 tabulates the reinforcement types and numbers as well as the short PP fiber volume ratio used to manufacture two medium capacity EPSs for each fiber ratio for the bending pull test. The cross-sectional shape and reinforcement type of the control EPS and newly proposed EPSs, including the medium capacity EPS, are shown in Fig. 2.

Reinforcement variations of newly proposed EPSs

The details of PS tendons, steel rebars, and the PP fiber ratio of the three tested specimens are tabulated in Table 5. As mentioned previously, PS forces of 510, 420, and 630 kN were applied to the light, medium, and heavy-capacity EPSs, respectively. The lower PS forces compared to the current EPSs sold on the market

Fig. 1. EPS specimen dimensions and geometry.

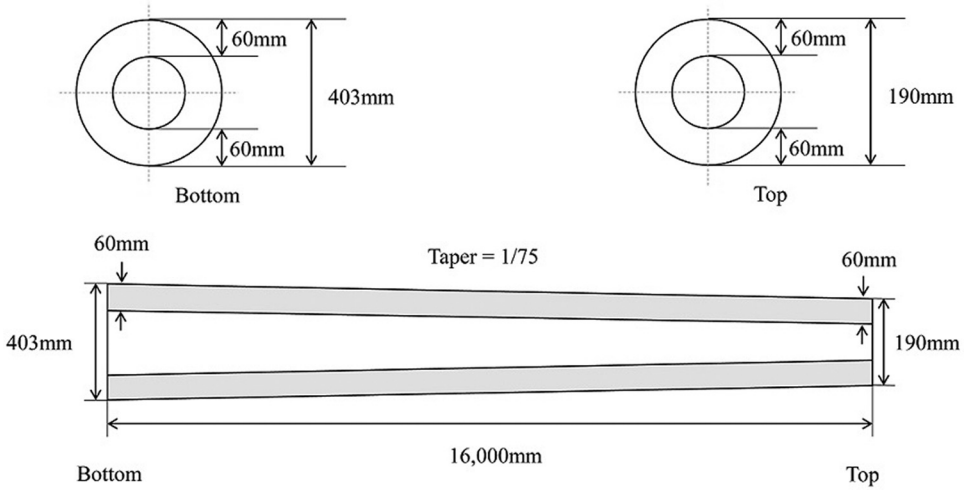

Table 2. Concrete mix proportion.

				Unit weight (kg/m^3)							
Type of EPS	f_{ck} (MPa)	W/B (%)	S/a (%)	W	C	FA	SF	S	G	SP	PP fiber vol. ratio
Light	80	25	42	143	526.2	—	45.76	764	1047	5.72	0.003
Medium	80	25	42	143	526.2	—	45.76	764	1047	5.72	0.003
Heavy	80	25	42	143	526.2	—	45.76	764	1047	5.72	0.003
Heavy	120	16	32	155	727	97	145	403	889	2.8	0.003

Note: FA, fly ash; SF, silica fume; SP, superplasticizer.

Table 3. Material properties of tendon and rebar.

Type	Product name	Yield strength (σ_y, MPa)	Tensile strength (σ_T, MPa)	Elastic modulus (E_s, MPa)
Tendon	SBPD-D-1	1275	1420	200 000
Rebar	SD700	910	1010	200 000

Table 4. PP fiber ratio of medium capacity EPS.

Specimen No.	Tendon size (mm)	No. used	Rebar size (mm)	No. used	PP fiber vol. ratio (30 mm PP fiber)
1	13	4	13	8	0.003
2	13	4	13	8	0.005
3	13	4	13	8	0.007

were due to the usage of PP FRC and the new reinforcement arrangements in the newly proposed EPSs. Even with the lower PS forces, the new EPSs have equivalent load carrying capacities as the current EPSs. Tendon diameter sizes of 11 mm and 13 mm were used for the light and medium/heavy EPSs, respectively. The total applied PS force was approximately 60–65% of the ultimate tensile strength of the tendon. Rebar diameter sizes of 11 mm and 13 mm were used for the light and heavy 2 specimens and the medium, heavy 1, heavy 2, and heavy u specimens, respectively. For spiral shear reinforcement, 3 mm steel wire with 9 cm spacing was used, which is equivalent to the current EPSs sold on the market. Korean Standard (KS F 4304 (Korean Standards Association 2015)) "Prestressed spun concrete poles" specifies the concrete strength of the pole to be over 49 MPa. The technical standard of concrete poles by Korea Electric Power Corporation (KEPCO) requires the concrete compressive strength to be 80 MPa or greater (Technical Standard of KEPCO 2006). In addition, according to KS F 2454 "Standard test method for compressive strength of spun concrete" (Korean Standards Association 2011), the test specimen for measuring the concrete compressive strength is manufactured using a hollow cylindrical mold with an outside diameter of 200 mm, a height of 300 mm, and a thickness of 40 mm. In this study, the 28 day concrete compressive strength was 80 MPa, except for the heavy u specimen as shown in Table 5. PS tendons and steel rebars used in the EPSs were in accordance with Korean Standard (KS D 3505 (Korean Standards Association 2019)) "Steel bars for prestressed concrete" and Korean Standard (KS D 3504 (Korean Standards Association 2016)) "Steel bars for concrete reinforcement", respectively. Dimensions of the new EPSs are the same as the dimensions of the current EPSs sold on the market.

Bending pull test method

The EPS bending pull test performed in this study followed the instructions of KS F 4304 "Prestressed spun concrete poles" (Korean Standards Association 2015). The schematic drawing of the test setup is shown in Fig. 3. The specimen was fixed by using two reaction plate grips, and then, a wire tensile force was applied at the tip of the pole until failure. An allowable crack width of 0.25 mm and a residual crack width limit of 0.05 mm after removal of the load were enforced. Generally, the ultimate failure load of the EPS is at least twice the design load. An incremental pulling load of 1 kN was applied until failure. The load and the load point deflection data were obtained from the load control box. Figure 4 shows the bending test photos.

Test results

Optimal fiber ratio test results

PP fiber volume ratios of 0.3%, 0.5%, and 0.7% were added to the trial concrete mix proportion used in manufacturing the medium-capacity EPS. As shown in Table 6 and Fig. 5, EPS mixed

Table 5. Tendon and rebar arrangements of new EPS specimens.

Capacity type	28 day conc. comp. st (MPa)	Tendon size (mm)	No. used	Rebar size (mm)	No. used	PP fiber vol. ratio
Light	80	11	6	11	6	0.003
Medium	80	13	4	13	8	0.003
Heavy 1	80	13	8	13	4	0.003
Heavy 2	80	13	8	11	6	0.003
Heavy 3	80	13	6	13	8	0.003
Heavy u	120	13	6	13	6	0.003

Fig. 2. Reinforcement variation type (control and newly proposed EPSs). [Colour online.]

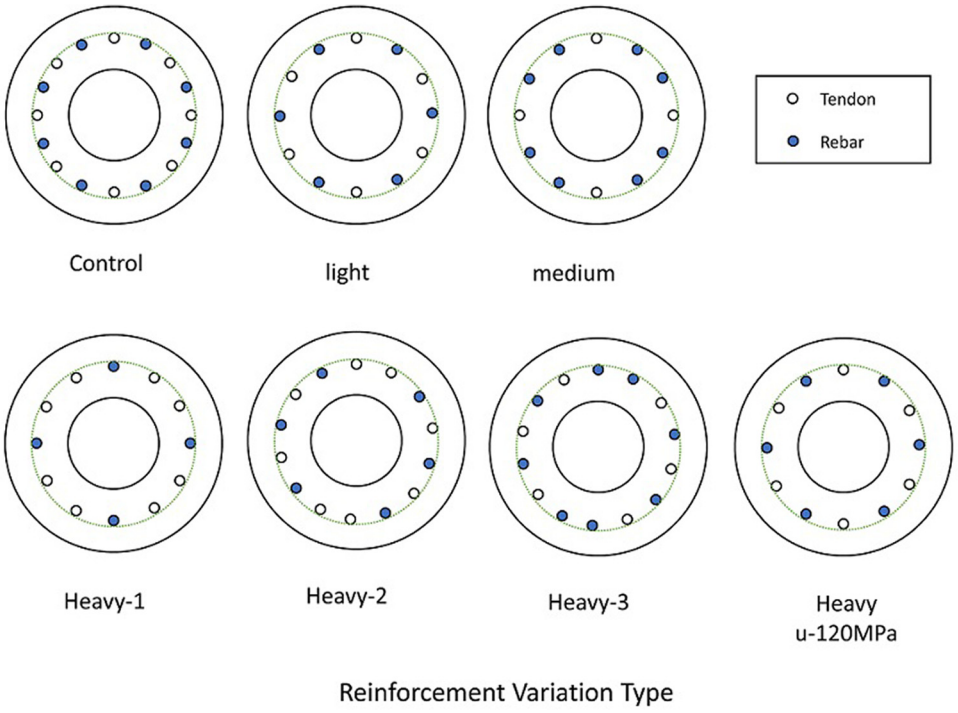

Fig. 3. Bending pull test setup. [Colour online.]

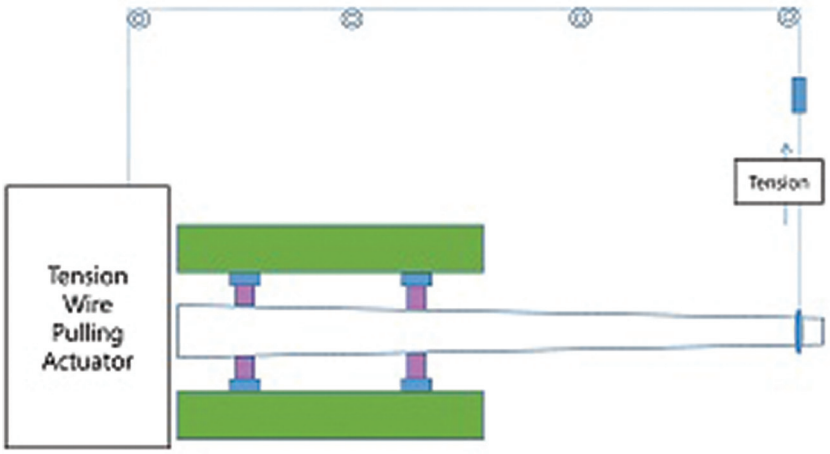

with the 0.3% fiber ratio demonstrated the largest bending load carrying capacity and deflection capacity. EPSs casted with the 0.3% fiber ratio shows 7% and 13.2% larger deflection rates than EPSs with 0.5% and 0.7% fiber ratio, respectively. Additionally, EPSs casted with the 0.3% fiber ratio showed 17.6% and 10.2% larger maximum applied loads than EPSs with the 0.5% and 0.7% fiber ratios, respectively. The superior performance of the 0.3% fiber ratio FRC EPS compared to 0.5% and 0.7% fiber ratio FRC

Fig. 4. Photos from bending pull test. [Colour online.]

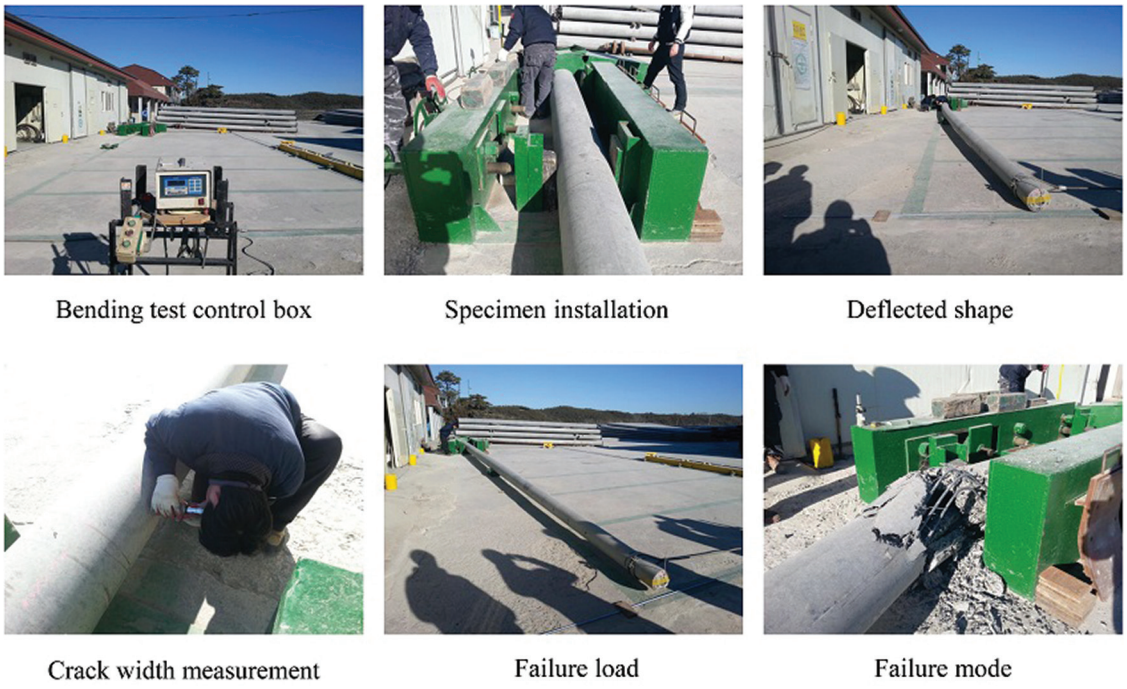

Table 6. Bending pull test results of EPSs with various PP fiber ratios.

Specimen	Fiber vol. ratio	Tendon size (mm)	No. used	Rebar size (mm)	No. used	7 kN cracking load		Failure load	
						Crack width (mm)	Deflection (mm)	Max. load (kN)	Deflection (mm)
Medium1	0.003	13	4	13	8	0.16	425	21	2990
Medium2	0.003	13	4	13	8	0.12	345	20.75	3000
Medium1	0.005	13	4	13	8	0.16	408	17.70	2870
Medium2	0.005	13	4	13	8	0.1	400	17.80	2710
Medium1	0.007	13	4	13	8	0.16	450	18.15	2620
Medium2	0.007	13	4	13	8	0.08	330	19.73	2670

EPSs is due to the fiber balling effect during FRC mixing. When a mixing ratio of 0.5% or 0.7% was used, fiber balling occurred during concrete mixing, causing an uneven distribution of fibers in the concrete during the spinning of EPS manufacturing. Figure 6 shows a photo of the fiber balling that occurred on the EPS surface. Conversely, when the concrete was mixed with a fiber ratio of 0.3%, no fiber balling occurred, and the fibers were evenly distributed throughout the member. From the bending test results of the load–deflection curves shown in Fig. 5, the concrete fiber ratio of 0.3% was the optimal ratio and was therefore used in the manufacturing of all EPS specimens in this study.

Korean standard design code of EPSs

KS F 4304 specifies design loads according to the type and dimensions of poles.

As mentioned in the introduction, this study used EPSs with 403 mm in bottom diameter and 190 mm in top diameter. The design loads of the EPSs are categorized into light, medium, and heavy, which can carry 5, 7, 10 kN, respectively (Table 7). When the design load is applied perpendicular to the EPS, the crack incidence width should not exceed 0.25 mm, and when the load is removed, no crack exceeding 0.05 mm in width should remain.

Results from light-capacity EPS test

The current and newly proposed light-capacity EPSs have 8/8 and 6/6 tendon/rebar reinforcements, respectively, with tendon/rebar diameters of 9.2 mm/8.0 mm and 11.0 mm/11.0 mm, respectively. The newly proposed light-capacity EPS has 2 fewer PS tendons and steel rebars than the current EPS. Table 8 and Fig. 7 show the bending test results of the current and newly proposed light-capacity EPSs. For a current light capacity EPS, when a pulling load reached the design load of 5 kN, no cracks were observed. However, when the load reached 7 kN, the EPS showed yielding. As shown in Fig. 4, the ultimate failure load was approximately 15 kN, or three times the design load of 5 kN. In the newly proposed EPS specimens, a similar failure behavior as seen in the current EPSs was observed; two fewer tendons and rebars were needed in these specimens thanks to the use of PP FRC.

Result from the medium-capacity EPS test

The current and newly proposed medium-capacity EPSs have 8/8 and 4/8 tendon/rebar ratios, respectively, with tendon/rebar diameters of 11.0/11.0 mm and 13.0/13.0 mm, respectively. Table 9 and Fig. 8 show the bending test results of the current and newly proposed medium-capacity EPSs. For the current medium-capacity EPS, when a load reached the cracking threshold of

Fig. 5. Load–deflection behavior results from medium EPS with various PP fiber ratios. [Colour online.]

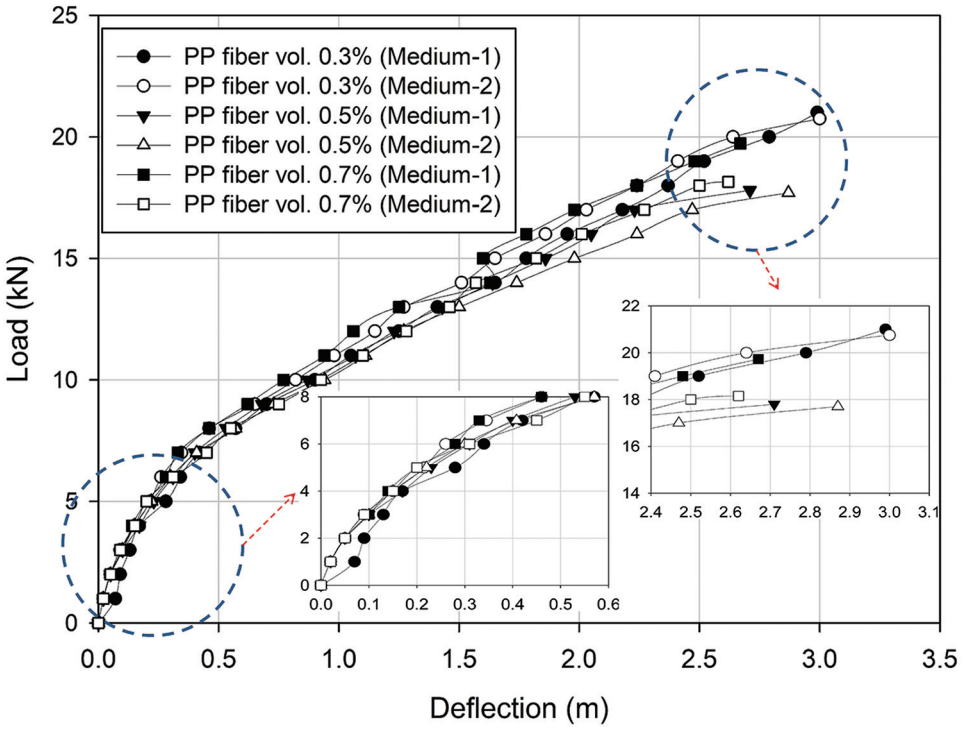

Fig. 6. Fiber transfer within EPS concrete. [Colour online.]

7 kN, no cracks were observed, but the new medium-EPSs did show cracks. However, the crack widths were less than the required limit of 0.25 mm (i.e., the crack width requirement of KS F 4304). However, the maximum tip deflection in the newly proposed EPS increased by more than 35% compared with that of the current EPS. The ultimate failure load of the new EPS was approximately 14% greater than that of the current EPS. The newly proposed medium-capacity EPS exhibited a 1.72-times larger maximum deflection at the ultimate load. As shown in Fig. 7, the yielding load of the new EPS was lower than that of the current EPS, but it showed more ductility due to the addition of the PP FRC. The current and new EPSs showed shattering catastrophic brittle failure (Fig. 9*a*) and ductile concrete intact cracking failure (Fig. 9*b*), respectively. The concrete intact ductile failure of the newly proposed EPS resulted from using fewer tendons and less PP FRC.

Table 7. Korean standard code design requirements of EPSs.

Length (mm)	Bottom diameter (mm)	Top diameter (mm)	Capacity type	Design load (kN)
16 000	403	190	Light	5
16 000	403	190	Medium	7
16 000	403	190	Heavy	10

Result from the heavy-capacity EPS test

The test results of the heavy-capacity EPSs are tabulated in Table 10. The table includes crack width/deflection and maximum load/deflection results at a cracking load of 10 kN and a failure load of 20 kN, respectively. All of the tendons and rebar diameter sizes were 13 mm. As shown in Table 7, no cracks were observed in the control, Heavy 1-1, and Heavy 2-1 specimens, while all other specimens had crack widths satisfying the 0.25 mm crack width requirement, except for the Heavy u-1 specimen.

The average load-point deflections of all the newly proposed heavy EPSs exceeded the deflection of the control heavy EPS at the crack load of 10 kN. The average maximum applied loads of the control and newly proposed heavy EPSs are, in order from smallest to largest, Heavy 2, Heavy u, control, Heavy 1, and Heavy 3. This result indicates that the newly proposed reinforcement combinations of 8 tendons with 4 rebars (Heavy 1) and 6 tendons with 8 rebars (Heavy 3) exceeded the control EPS's load carrying capacity. The load-point deflections of the newly proposed heavy EPSs exceeded the control heavy EPS deflection except for the Heavy 2-3 specimen, thus indicating vast improvement through using PP FRC and new reinforcement arrangements.

Table 8. Bending pull test results of light-capacity EPSs.

Specimen	Tendon size (mm)	No. used	Rebar size (mm)	No. used	5 kN cracking load		Failure load	
					Crack width (mm)	Deflection (mm)	Max. load (kN)	Deflection (mm)
Control Light	9.2	8	8	8	No	185	16.65	2700
Light-1	11	6	11	6	No	170	16.25	2740
Light-2	11	6	11	6	No	180	14.80	2350

Fig. 7. Load–deflection behavior results from light-capacity EPSs. [Colour online.]

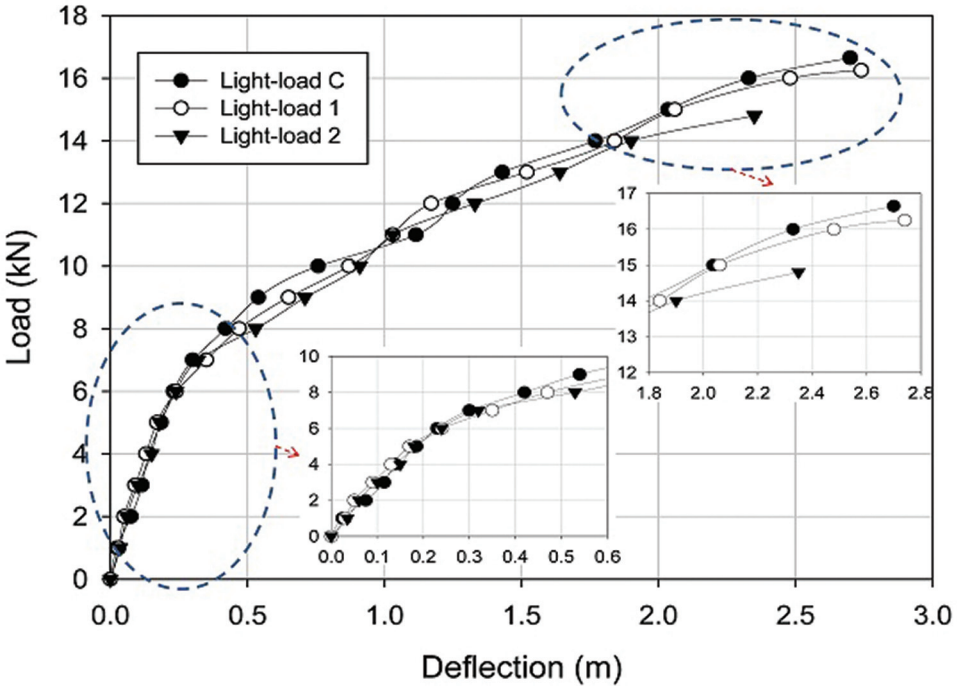

Table 9. Bending pull test results of medium-capacity EPSs.

Specimen	Tendon size (mm)	No. used	Rebar size (mm)	No. used	7 kN cracking load		Failure load	
					Crack width (mm)	Deflection (mm)	Max. load (kN)	Deflection (mm)
Control Medium	11	8	11	8	No	255	16.70	1740
Medium-1	13	4	13	8	0.16	425	21	2990
Medium-2	13	4	13	8	0.12	345	20.75	3000
Medium-3	13	4	13	8	0.16	430	19.10	3020

Figures 10, 11, 12, 13, and 14 show the load–deflection curves of heavy EPSs with various tendon and rebar reinforcement combinations. All of the load–deflection graphs show overall ranges, including magnified results of the elastic and ultimate failure ranges. As illustrated in all the figures, the control and newly proposed heavy EPSs show similar behaviors within the elastic range. However, once the yielding occurred, the control EPS had a slightly higher stiffness than the new EPSs. At the ultimate failure range, the new EPSs had larger deflections than the control EPS. Since the area under the load–deflection curve is equivalent to the energy absorbing capacity of EPS, the larger deflections with the higher load carrying capacities of the Heavy 1 and Heavy 3 EPSs would have a higher resistance to instantaneous high velocity impacts or wind gust loading.

Conclusions

This study focused on the bending performance of the newly proposed EPS structures applied with various tendon and rebar arrangements, as well as with PP FRC, to convert EPS failure behavior from brittle to ductile. Based on the findings, the following conclusions are drawn.

(1) Based on the load–deflection curve from the bending test results, the concrete fiber ratio of 0.3% proved to be optimal. EPSs mixed with the 0.3% fiber ratio showed 7% and 13.2% larger deflection rates than EPSs with 0.5% and 0.7% fiber ratios, respectively. Moreover, EPSs casted with the 0.3% fiber ratio displayed 17.6% and 10.2% larger maximum applied loads than EPSs with the 0.5% and 0.7% ratios, respectively.

Fig. 8. Load–deflection behavior results from medium-capacity EPSs. [Colour online.]

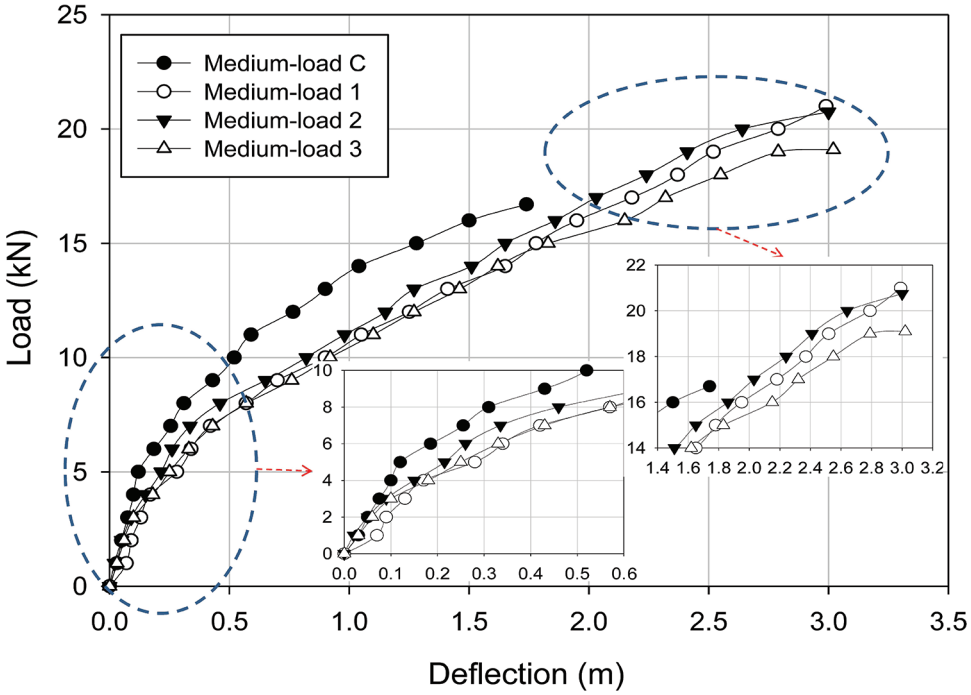

Fig. 9. Comparison of brittle and ductile failure behavior: (*a*) current EPS and (*b*) new EPS. [Colour online.]

Table 10. Bending pull test results of heavy-capacity EPSs.

					10 kN cracking load		Failure load			
Specimen	Tendon size (mm)	No. used	Rebar size (mm)	No. used	Crack width (mm)	Deflection (mm)	Max. load (kN)		Deflection at 20 kN (mm)	
Control Heavy	13	8	13	8	No	370	20.20		1700	
Heavy 1-1	13	8	13	4	No	390	21.25	Avg. 20.78	2340	Avg. 2227
Heavy 1-2	13	8	13	4	0.08	395	20.30		2100	
Heavy 1-3	13	8	13	4	0.06	405	20.80		2240	
Heavy 2-1	13	8	13	6	No	420	20.70	Avg. 18.98	1900	Avg. 1813
Heavy 2-2	13	8	13	6	0.12	480	19.40		1900	
Heavy 2-3	13	8	13	6	0.16	470	16.85		1640	
Heavy 3-1	13	6	13	8	0.1	490	22.10	Avg. 21.73	2270	Avg. 2210
Heavy 3-2	13	6	13	8	0.12	460	21.45		2130	
Heavy 3-3	13	6	13	8	0.12	455	21.65		2230	
Heavy u-1 120 MPa	13	6	13	6	0.26	615	18.70	Avg. 19.05	2320	Avg. 2350
Heavy u-2 120 MPa	13	6	13	6	0.24	535	18.70		2300	
Heavy u-3 120 MPa	13	6	13	6	0.16	525	19.75		2430	

Fig. 10. Load–deflection behavior results from heavy-capacity EPSs with 80 MPa FRC (Heavy 1: 8 tendons, 4 rebars, f_{ck} = 80 MPa). [Colour online.]

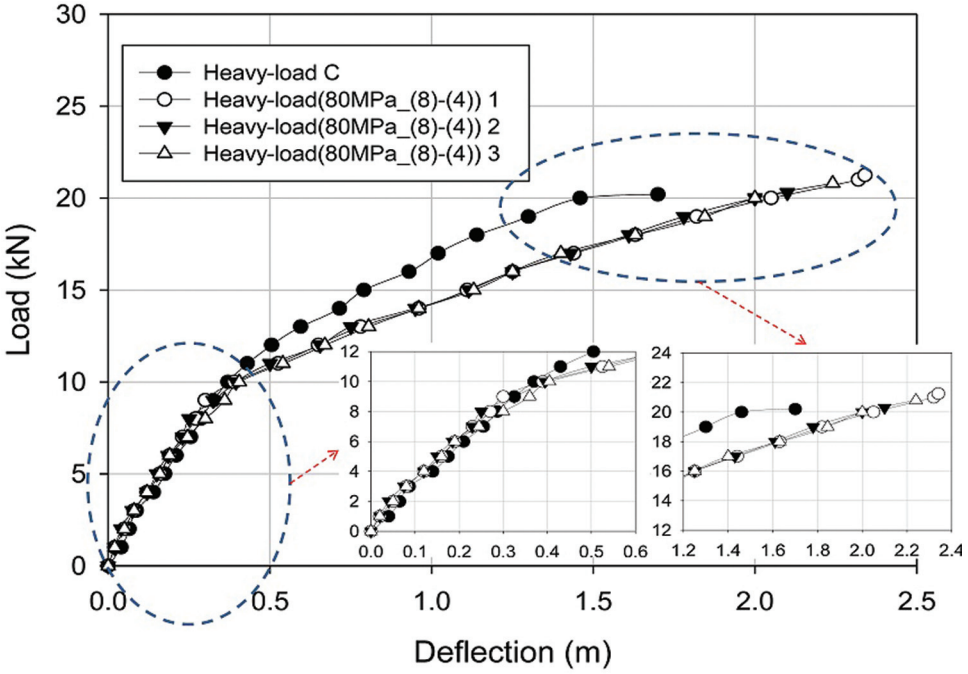

Fig. 11. Load–deflection behavior results from heavy-capacity EPSs with 80 MPa FRC (Heavy 2: 8 tendons, 6 rebars, f_{ck} = 80 MPa). [Colour online.]

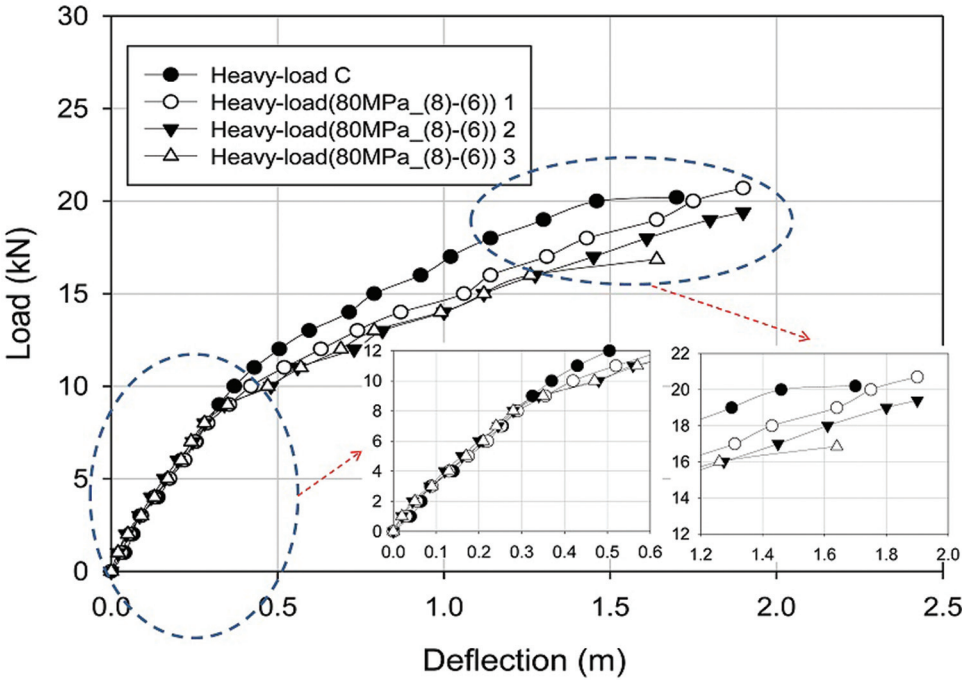

(2) In a comparison of the current and newly proposed light capacity EPS, the ultimate failure load was approximately 15 kN, or three times the design load of 5 kN. In the newly proposed EPS specimens, a similar failure behavior as seen in current EPSs was observed; two fewer tendons and rebars were needed in these specimens owing to the use of PP FRC.

(3) In a comparison of the current and newly proposed medium-EPSs, the maximum tip deflection in the new EPS was more than 35%

Fig. 12. Load–deflection behavior results from heavy-capacity EPSs with 80 MPa FRC (Heavy 3: 6 tendons, 8 rebars, f_{ck} = 80 MPa). [Colour online.]

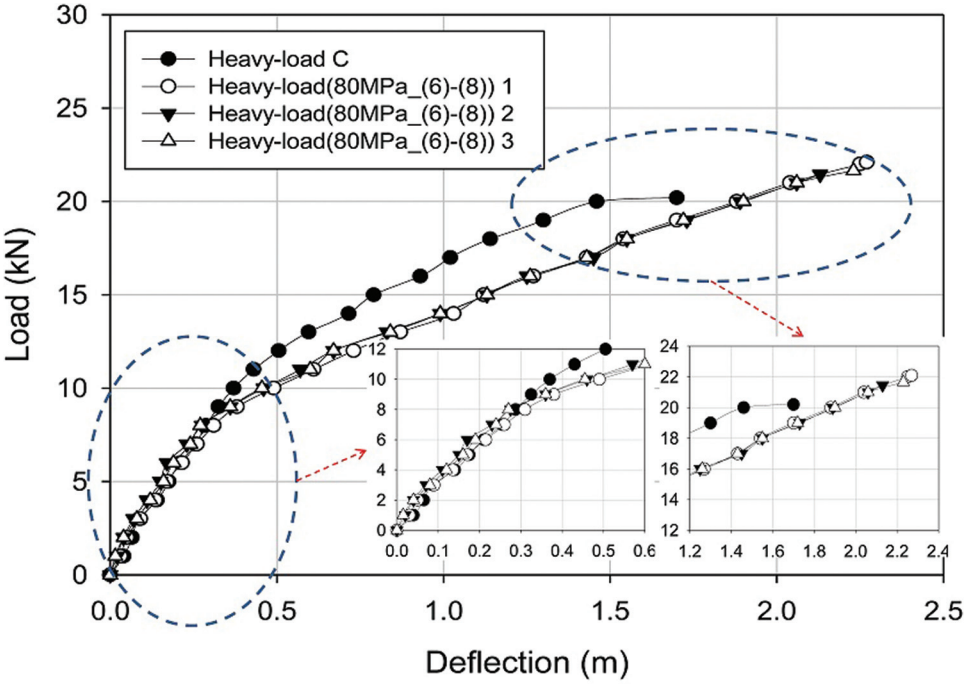

Fig. 13. Load–deflection behavior results from heavy-capacity EPSs with 120 MPa FRC (Heavy u: 6 tendons, 6 rebars, f_{ck} = 120 MPa). [Colour online.]

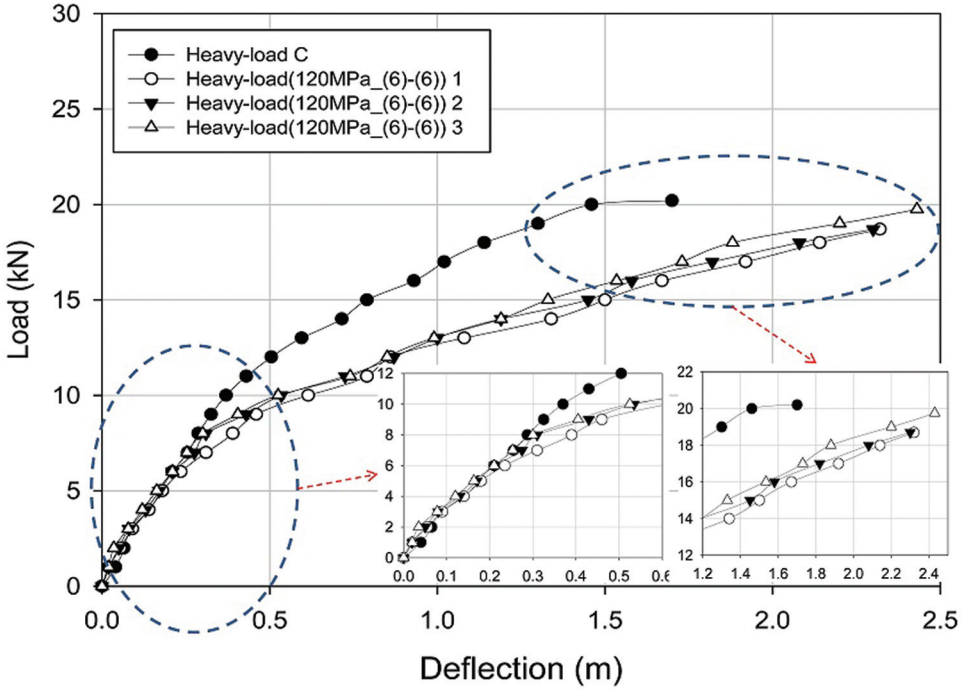

higher than that of the current EPS. The ultimate failure load of the new EPS was approximately 14% greater than that of the current EPS.

(4) The average load-point deflections of all newly proposed heavy EPSs exceeded the deflection of the control heavy EPS at the cracking load of 10 kN. The average maximum applied loads of the control and the newly proposed heavy EPSs indicated that the newly proposed reinforcement combinations of 8 tendons with 4 rebars (Heavy 1) and 6 tendons with 8 rebars (Heavy 3)

Fig. 14. Average load–deflection behavior results from heavy-capacity EPSs. [Colour online.]

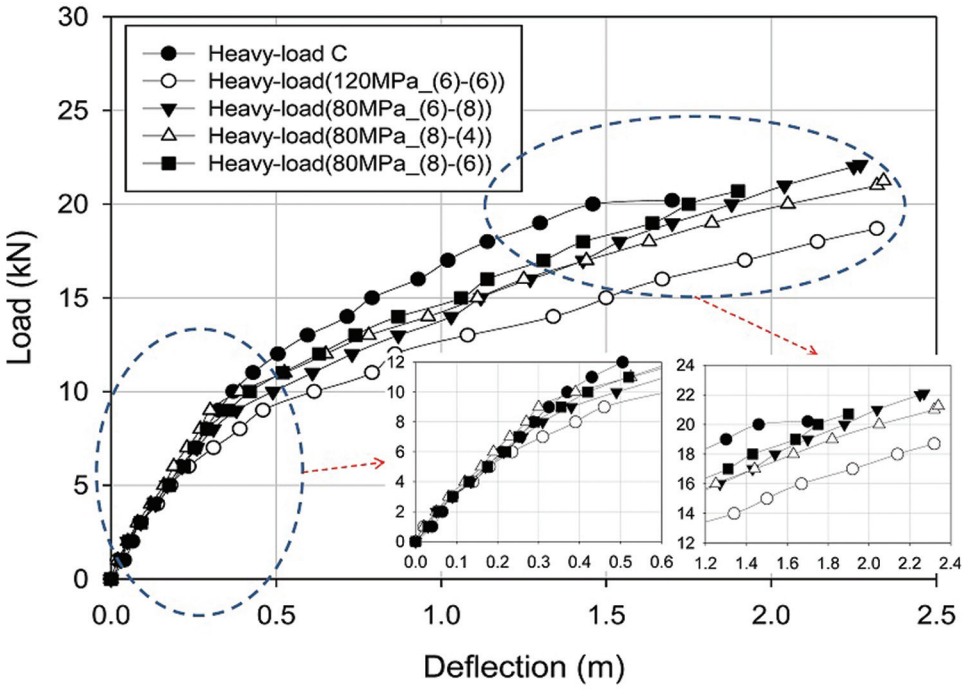

exceeded the control's EPS load carrying capacity. At the ultimate failure range, the new EPSs have larger deflection rates than the control EPS.

Acknowledgements

This work was supported by the National Research Foundation of Korea (NRF) grant funded by the Korea government (MSIP) (No. 2016R1A2B3009444); the Nuclear Safety Research Program, through the Korea Foundation of Nuclear Safety (KOFONS), granted financial resources from the Nuclear Safety and Security Commission (NSSC), Republic of Korea (No. 1403010).

References

Ali, F., Nadjai, A., and Choi, S. 2010. Numerical and experimental investigation of the behavior of high strength concrete columns in fire. Engineering structures, **32**(5): 1236–1243. doi:10.1016/j.engstruct.2009.12.049.

Arya, C., and Darko, F.K.O. 1996. Influence of crack frequency on reinforcement of corrosion in concrete. Cement and Concrete Research, **26**(3): 345–353. doi:10.1016/S0008-8846(96)85022-8.

Audenaert, K., Marsavina, L., and Schutter, G.D. 2009. Influence of cracks on the service life of concrete structures in a marine environment. Key Engineering Materials, **399**: 153–160. doi:10.4028/www.scientific.net/KEM.399.153.

Castoldi, R.D.S., Souza, L.M.S.D., and de Andrade Silva, F. 2019. Comparative study on the mechanical behavior and durability of polypropylene and sisal fiber reinforced concretes. Construction and Building Materials, **211**: 617–628. doi:10.1016/j.conbuildmat.2019.03.282.

Hwang, J.H., Lee, D.H., Ju, H., Kim, K.S., Kang, T.H.K., and Pan, Z. 2016. Shear deformation of steel fiber-reinforced prestressed concrete beams. International Journal of Concrete Structures and Materials, **10**(3): 53–63. doi:10.1007/s40069-016-0159-2.

Janke, L., Czaderski, C., Ruth, J., and Motavalli, M. 2009. Experiments on the residual load-bearing capacity of prestressed confined concrete columns. Engineering Structures, **31**(10): 2247–2256. doi:10.1016/j.engstruct.2009.04.006.

Jung, K.H., Yi, N.H., and Kim, J.H.J. 2010. Structural safety and serviceability evaluations of prestressed concrete hybrid bridge girders with corrugated or steel truss web members. Engineering Structures, **32**(12): 3866–3878. doi:10.1016/j.engstruct.2010.08.029.

Kim, S.B., Kim, J.H.J., Kim, T.K., and Eoh, C.S. 2010. Behavior of hollow box girder using unbonded compressive pre-stressing. KSCE, **30**(3A): 201–209. [In Korean.]

Korean Standards Association. 2011. KS F 2454. Standard test method for compressive strength of spun concrete. Korean Standards Association.

Korean Standards Association. 2015. KS F 4304. Prestressed spun concrete poles. Korean Standards Association.

Korean Standards Association. 2016. KS D 3504. Steel bars for concrete reinforcement. Korean Standards Association.

Korean Standards Association. 2019. KS D 3505. Steel bars for prestressed concrete. Korean Standards Association.

Lee, W.K., and Billington, S. 2007. Simulation and performance-based earthquake engineering assessment of self-centering post-tensioned concrete bridge systems. Ph.D. thesis, Stanford University.

Nathan, N.D. 1985. Rational analysis and design of prestressed concrete beam columns and wall panels. PCI Journal, **30**(3): 82–133. doi:10.15554/pcij.05011985.82.133.

Phan, D.H., Kim, J.H.J., Yi, N.H., You, Y.J., and Kim, J.W. 2012. Strength targeted PBMD of HSC based on one-parameter Bayesian probabilistic method. Journal of Advanced Concrete Technology, **10**(4): 137–150. doi:10.3151/jact.10.137.

Rodriguez-Gutierrez, J.A., and Aristizabal-Ochoa, J.D. 2001*a*. Reinforced, partially, and fully prestressed slender concrete columns under biaxial bending and axial load. Journal of Structural Engineering, **127**(7): 774–783. doi:10.1061/(ASCE)0733-9445(2001)127:7(774).

Rodriguez-Gutierrez, J.A., and Aristizabal-Ochoa, J.D. 2001*b*. M-P-φ diagrams for reinforced, partially, and fully prestressed concrete sections under biaxial bending and axial load. Journal of Structural Engineering, **127**(7): 763–773. doi:10.1061/(ASCE)0733-9445(2001)127:7(763).

Saatcioglu, M., and Yalcin, C. 2003. External prestressing concrete columns for improved seismic shear resistance. Journal of Structural Engineering, **129**(8): 1057–1070. doi:10.1061/(ASCE)0733-9445(2003)129:8(1057).

Shanaka, K.P., Mendis, P., Ngo, T., Portella, J., and Nguyen, K. 2018. Understanding failure and stress-strain behavior of very-high strength concrete (>100 MPa) confined by lateral reinforcement. Construction and Building Materials, **189**: 55–77. doi:10.1016/j.conbuildmat.2018.08.192.

Soltani, A., Harries, K.A., and Shahrooz, B.M. 2013. Crack opening behavior of concrete reinforced with high strength reinforcing steel. International Journal of Concrete Structures and Materials, **7**(4): 253–264. doi:10.1007/s40069-013-0054-z.

Technical Standard of KEPCO (ES 102-128-619). 2006. Concrete poles.

Thompsin, K., and Park, R. 1980. Ductility of prestressed and partially prestressed concrete beam sections. PCI Journal, **25**(2): 47–69. Available from https://pdfs.semanticscholar.org/5ff7/0d34136d2fdd74a2cd13bfd31b0b7e301f61.pdf.

Vivek, B., Sharma, S., Raychowdhury, P., and Ray-Chaudhri, S. 2017. A study on failure mechanism of self-supported electric poles through full-scale field

testing. Engineering Failure Analysis, **77**: 102–117. doi:10.1016/j.engfailanal.2016.12.019.

Wolanski, A.J. 2004. Flexural behavior of reinforced and prestressed concrete beams using finite element analysis. Ph.D. thesis, Faculty of the Graduate School, Marquette University.

Xi, X., Yang, S., and Li, C.Q. 2018. Accurate cover crack modelling of reinforced concrete structures subjected to non-uniform corrosion. Structure and Infrastructure Engineering, **14**(12): 1628–1640. doi:10.1080/15732479.2018.1486440.

Xu, L., Li, B., Ding, X., Chi, Y., Li, C., Huang, B., and Shi, Y. 2018. Experimental investigation on damage behavior of polypropylene fiber reinforced concrete under compression. International Journal of Concrete Structures and Materials, **12**(7): 1007–1026. doi:10.1186/s40069-018-0302-3.